Noise performance of magneto-inductive cables

M. C. K. Wiltshire and R. R. A. Syms

Citation: Journal of Applied Physics **116**, 034503 (2014); doi: 10.1063/1.4890308
View online: http://dx.doi.org/10.1063/1.4890308
View Table of Contents: http://scitation.aip.org/content/aip/journal/jap/116/3?ver=pdfcov
Published by the AIP Publishing

Noise performance of magneto-inductive cables

M. C. K. Wiltshire[a] and R. R. A. Syms
Optical and Semiconductor Devices Group, Department of Electrical and Electronic Engineering, Imperial College London, Exhibition Road, London SW7 2AZ, United Kingdom

(Received 21 May 2014; accepted 3 July 2014; published online 16 July 2014)

Magneto-inductive (MI) waveguides are metamaterial structures based on periodic arrangements of inductively coupled resonant magnetic elements. They are of interest for power transfer, communications and sensing, and can be realised in a flexible cable format. Signal-to-noise ratio is extremely important in applications involving signals. Here, we present the first experimental measurements of the noise performance of metamaterial cables. We focus on an application involving radiofrequency signal transmission in internal magnetic resonance imaging (MRI), where the subdivision of the metamaterial cable provides intrinsic patient safety. We consider MI cables suitable for use at 300 MHz during ^{1}H MRI at 7 T, and find noise figures of 2.3–2.8 dB/m, together with losses of 3.0–3.9 dB/m, in good agreement with model calculations. These values are high compared to conventional cables, but become acceptable when (as here) the environment precludes the use of continuous conductors. To understand this behaviour, we present arguments for the fundamental performance limitations of these cables. © *2014 AIP Publishing LLC*.
[http://dx.doi.org/10.1063/1.4890308]

I. INTRODUCTION

Electromagnetic induction was first investigated by Faraday in 1831 and is embodied in Faraday's Law, $\nabla \times \mathbf{E} = -\partial \mathbf{B}/\partial t$, relating the spatial variation of the induced electric field to the rate of change of a magnetic field. The principle was proposed for power transfer by Tesla in the 1890s,[1] and has recently been further developed.[2] It has also been considered for communications in challenged environments (underground or undersea), where electromagnetic waves are strongly attenuated.[3] The key problem with free space magneto-inductive (MI) systems is the rapid fall-off in coupling efficiency with distance, which limits the useful range to approximately the coil diameter. One solution is the introduction of additional resonant loops between the transmitter and receiver.[4,5] When there are many such loops, these systems can be considered an MI waveguide[6–8] or, in the limit, a metamaterial.

Metamaterials are artificial media,[9–11] whose electromagnetic properties are determined not by their chemistry, but by their structure: in particular, arrays of ring resonators[11,12] or of "Swiss Rolls"[11,13] can provide an effective magnetic response in the radiofrequency (RF) and microwave regions. As in any periodic system, waves can propagate if the elements are coupled. For magnetic metamaterials, which are inductively coupled, these are MI waves, which are analogous to spin-waves or magnons[14] in conventional magnetic materials. MI waves were proposed in Refs. 6 and 7, verified experimentally in Refs. 15 and 16, and have been widely studied ever since. Practical MI devices have been developed,[17] and studies have been made of communication systems[4,18,19] based on two and three dimensional waveguides.

Generally, the elements are spatially isolated resonant loops, so the magnetic coupling is weak. An alternative approach is to form the loops on a flexible substrate as the elements of a cable.[20] Using double-sided patterning, the loops can be overlaid to enhance their coupling, and thus form cables that have low loss and are insensitive to bending.[21] MI cables are potentially useful as safe interconnects to internal coils in magnetic resonance imaging (MRI). A small internal coil can have a better filling factor for the target tissue but a smaller sensitivity to body noise, resulting in an improved signal-to-noise ratio (SNR) compared to external coils. Unfortunately, transmission of the signal using continuous wires is inherently dangerous, because standing waves may easily be excited on long conductors during the excitation phase of MRI. If this occurs, rapid heating ensues. MI waveguide cables, on the other hand, have no continuous electrical paths, and so are inherently MRI-safe.[20,22] They can be wrapped around a catheter and are compatible with procedures such as endoscopic insertion.[22,23]

Key issues in communication, imaging, and sensing are loss and noise. In MI waveguides, loss arises from the finite resistance of the conductors (typically copper) used to construct the LC resonators. This resistance generates thermal noise, as originally observed and explained by Johnson and Nyquist in the 1920s.[24,25] This linkage is fundamental and was later developed into the fluctuation-dissipation theorem (FDT),[26–28] which relates fluctuations (or noise) to loss (or the imaginary part of the susceptibility). At low frequency, the mean square noise voltage from a resistor R at a temperature T is given by[24,25]

$$\langle V_n^2 \rangle = 4k_B TR \tag{1}$$

per unit bandwidth, where k_B is Boltzmann's constant. Introducing sources mimicking thermal noise generation into the circuit model for MI waveguides allows a detailed prediction of the noise performance.[29,30] A similar approach has been used[19,31] to study MI communication systems.

[a]Author to whom correspondence should be addressed. Electronic mail: michael.wiltshire@imperial.ac.uk

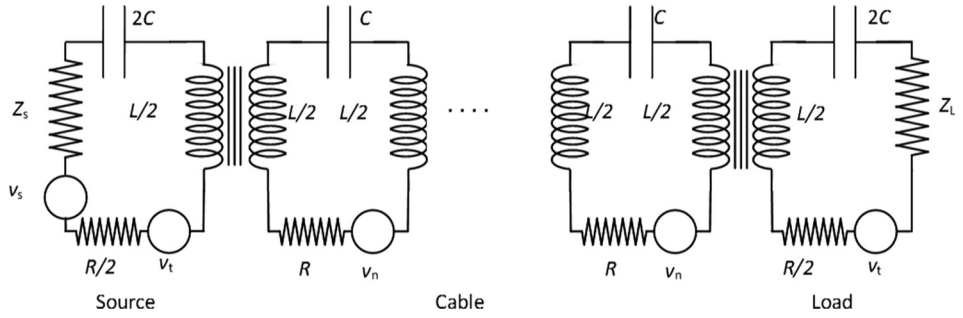

FIG. 1. The circuit model for an MI cable consists of a series of loops containing inductors, L (shown here as two elements of $L/2$ in series) and their associated resistors, R, and capacitors, C. The loops are coupled through a mutual inductance M. The terminations comprise half-loops with inductance $L/2$, resistance $R/2$, and capacitance $2C$, to act as broadband couplers to the source or load. The source has a voltage v_s and impedance Z_s, and the load an impedance Z_L. Each resistance in the cable has an associated noise voltage v_n and those in the terminations have v_t.

In a previous paper,[32] we investigated the noise in coupled resonator arrays. Noise was generated by the resistance of the copper tracks, according to (1), but trapped within the array. Consequently, in extended samples, it took the form of standing waves. These noise resonances were probed and the measurements compared to the predictions of a simple circuit model, with excellent agreement. Here, we study the noise that is coupled *out* of an array, which is now configured as a practical interconnect based on a MI cable, and present the first experimental measurement of the noise performance of such cables. In Sec. II, we develop an appropriate circuit model. In Sec. III, we describe the experimental cables and compare measurements of their transmission and noise figure with model predictions. In Sec. IV, we contrast the performance of MI cables with more conventional cables and discuss their fundamental limitations. Finally, we present conclusions in Sec. V.

II. CIRCUIT MODEL

The model is simple: the cable and its terminations are described by their circuit parameters, including those of the source and load, as shown schematically in Figure 1.

The characteristic impedance of an MI waveguide is[33]

$$Z_{0MI} = j\omega_0 M \exp(-jka), \tag{2}$$

where ω_0 is the angular resonant frequency, M is the mutual inductance between nearest neighbours, $k = k' - jk''$ is the complex propagation coefficient, and a is the unit cell length. This impedance is generally complex, but at resonance, $k'a = \pi/2$ and $k''a \approx 1/\kappa Q$, so for low loss (high Q) systems, the impedance reduces to $Z_{0MI} = \omega_0 M$, which is purely resistive. It is therefore possible, by careful choice of parameters, to match the cable to 50 Ω impedance for connection to conventional RF systems. Furthermore, by using broadband terminations comprising loops with half the inductance and double the capacitance of the main cable,[34] a reasonable match can be achieved over the whole operating band. These terminations, with a source of voltage v_s and impedance Z_s and a load of impedance Z_L, are shown in Fig. 1. Noise is modelled by providing each resistive element with a voltage source whose value is chosen to represent its Johnson noise (1). These sources are uncorrelated.

We then apply Kirchhoff's circuit equations to calculate the internal currents and hence the voltage that appears across the load. In matrix form these are

$$\begin{pmatrix} Z_s+Z_t & j\omega M_t & 0 & \cdots & \cdots & \cdots & 0 \\ j\omega M_t & Z & j\omega M & \cdots & \cdots & \cdots & \vdots \\ 0 & j\omega M & Z & \cdots & \cdots & \cdots & \vdots \\ \vdots & \vdots & \vdots & \ddots & \cdots & \cdots & \vdots \\ \vdots & \vdots & \vdots & \vdots & Z & j\omega M & 0 \\ \vdots & \vdots & \vdots & \vdots & j\omega M & Z & j\omega M_t \\ 0 & \cdots & \cdots & \cdots & 0 & j\omega M_t & Z_L+Z_t \end{pmatrix} \begin{pmatrix} I_0 \\ I_1 \\ I_2 \\ \vdots \\ I_{N-1} \\ I_N \\ I_t \end{pmatrix} = \begin{pmatrix} \sqrt{v_s^2+v_t^2} \\ v_n \\ v_n \\ \vdots \\ v_n \\ v_n \\ v_t \end{pmatrix}, \tag{3}$$

where $Z_t = j\omega L/2 + R/2 + 1/j\omega 2C$ and $Z = j\omega L + R + 1/j\omega C$ are the impedance of the terminating and cable loops, respectively, $M = \kappa L/2$ is the mutual inductance between loops in the cable body, and $M_t = \kappa L/\sqrt{2}$ that at the terminations. Here, $\kappa = 2M/L$ is the inter-loop coupling coefficient used in normalised descriptions. The source and load impedances

(Z_s and Z_L, respectively) are both set to 50 Ω here. The noise voltage in the source loop is the incoherent sum of the noise (v_s) from the source itself and the noise voltage (v_t) arising from the resistance in the loop, according to (1). The noise of the load impedance is not included in this calculation; it is incorporated in the noise characteristics of the succeeding instrument. Then, (3) can be written as $\mathbf{ZI}=\mathbf{V}$ or $\mathbf{I}=\mathbf{Z}^{-1}\mathbf{V}=\mathbf{YV}$, where $\mathbf{Z}$ and $\mathbf{Y}=\mathbf{Z}^{-1}$ are the impedance and admittance matrices, respectively. The contributions of the source and each of the cable loops to the noise current in the output circuit, I_t, (and hence to the noise voltage in the load), are calculated independently, and summed incoherently. Thus, the noise in the load is

$$v^2 = \left|Y_{N+2,1}\sqrt{v_s^2 + v_t^2}Z_0\right|^2 + \sum_{n=1}^{N}|Y_{N+2,n+1}v_nZ_0|^2 + |Y_{N+2,N+2}v_tZ_0|^2. \quad (4)$$

The cable transmission can also be obtained from (3), but with all the noise voltages set to zero, and a signal voltage V_s of unity. This gives

$$G = Y_{N+2,1}\cdot V_s\cdot Z_0, \quad (5)$$

where we have written the transmission as G to correspond with the notation used for the noise figure derivation below.

The noise factor, F, and noise figure, NF, for a device under test are defined as

$$F = SNR_{in}/SNR_{out} \quad \text{and} \quad NF = 10\log_{10}(F). \quad (6)$$

Here, SNR_{in} is the signal-to-noise ratio at the device input, and SNR_{out} is the corresponding value at the output. Let the input signal and noise be S and N_i, respectively, and let the device (the cable) have a gain or transmission G and generate additive noise N_A at its output. Then

$$F = \frac{S/N_i}{GS/(GN_i+N_A)} = \frac{GN_i+N_A}{GN_i} = 1+\frac{N_A}{GN_i}, \quad (7)$$

N_A can be obtained from (4), N_i from (1), and G from (5), thus allowing the noise figure to be calculated from the circuit parameters.

III. MEASUREMENTS

The experimental samples consisted of two cables from a test set designed to explore performance around 300 MHz, compatible with ^{1}H MRI at 7 T, with the key difference between them being the size and number of the inductive loops, and hence the mutual inductance between the loops. The cables used here contained 9 and 10 loops of 80 and 70 mm length, respectively, so that each cable was ~85 cm long. The cables were fabricated in copper-clad Kapton® flexible printed circuit board (PCB) (35 μm Cu on 25 μm polyimide; Dupont) by a double-sided patterning process,[35] with the layout shown in Figure 2(a).

Each loop is divided into two halves, each of inductance L/2, and the capacitors are similarly divided into two, each of value 2C. The loops are overlaid, with neighbouring loops on opposite sides of the substrate, to maximise the desired coupling while rendering the coupling to non-nearest neighbours negligible. The tracks on the two sides of the substrate are off-set to reduce parasitic capacitance (which has the effect of lowering the high frequency cut-off of the cables and increasing attenuation through the dielectric loss of the Kapton).[36] The processed PCB (Figure 2(b)) contained arrays of cables together with single and paired elements used to extract the electrical parameters. The patterned cables were first separated and each loop made resonant using surface mount capacitors, and then terminated to match to 50 Ω over the operating band using transducer final loops with inductance $L/2$ and capacitance $2C$ (Ref. 34) (Figure 2(b), inset, shows a completed cable). Table I shows the details of the cables.

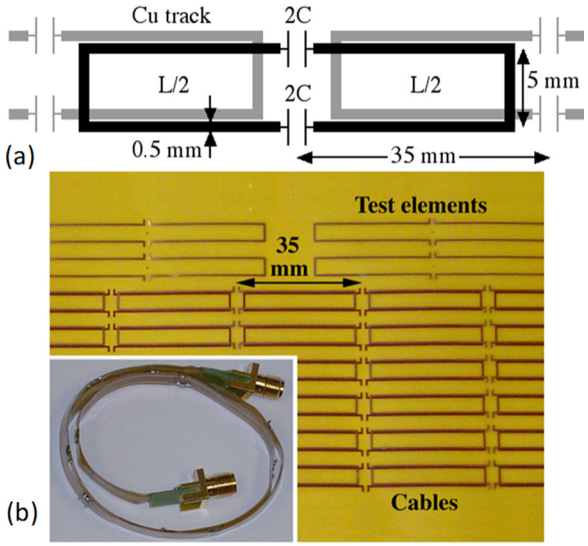

FIG. 2. (a) The layout and (b) the processed flexible circuit board for cable 2 (see Table I). The inset to (b) shows the completed cable with terminations.

A. Electrical parameters

The electrical parameters in Table I were measured as follows. The self inductance of the loops was found by measuring the resonant frequency of a single element, tuned with a known capacitance, using weakly coupled inductive probes for excitation and detection, and the Q-factor was obtained from the full width at half height of this resonance. The mutual inductance, and hence the coupling coefficient, was found from the resonant frequencies of a coupled pair of loops. Hence the characteristic impedance could also be determined. The cables were then characterised by measuring their S-parameters. Each cable was mounted in turn in a screened enclosure, 85 cm long × 15 cm square, made from unprocessed rigid PCB (single sided 1 oz copper on FR4), with an SMA (Sub-Miniature version A connector) lead-through at each end. This enclosure was placed centrally within a further enclosure of similar construction, with overall dimensions 90 × 45 × 30 cm. The S-parameters were measured using an Agilent 8753ES network analyser, whose ports were calibrated with open, short and load

TABLE I. Physical and electrical parameters for the MI cables.

Cable	Loop length (mm)	No of loops[a]	Loop inductance (nH)	Additional capacitance (pF)	Quality factor, Q	Resonant frequency (MHz)	Coupling coefficient κ	Frequency band (MHz)	Z_{0MI} (Ω)
1	80	9 + 2	118.4	5.1	110	204.7	0.66	159–351	49.7
2	70	10 + 2	104.1	4.7	120	227.5	0.65	177–384	48.6

[a]Shown as the number of loops in the cable +2 terminating loops.

attachments in place of the test sample, together with a through connection comprising a suitable SMA adaptor. All four S-parameters were measured; the measured S_{21} spectra are shown as the red full lines in Figure 3, and compared to the spectra calculated using the currents derived from (3) and the parameters of Table I, shown as the blue, dashed-dotted lines: this gives a reasonably satisfactory description of the cable behaviour. The major differences are that the measured pass band is wider and lower than the calculated pass band. These arise primarily from small variations in the patterning of the tracks, so that adjacent loops in the cables have less off-set than those in the test areas. This leads to a larger coupling coefficient and also to increased parasitic capacitance, which in turn increases loss from the dielectric substrate. We have not attempted to model these in detail, but have empirically included their effects in the model. Thus, we have introduced an extra capacitance, typically 0.5 pF, in the loops, and allowed it to be lossy: i.e., we have written $\Delta C = \Delta C_0(1+\delta)$, with δ in the range of 0.1–0.25. (Note that this is not a true reflection of the loss tangent of the substrate, but embraces all the parasitic loss contributions). We have also adjusted the coupling parameter κ to ~0.69, which gives a better match to the bandwidth. The spectra calculated with these parameters are shown as the green dashed lines in Figure 3 and give a good representation of the measured data.

B. Noise figure

The conventional method for measuring noise figure is to use a switchable noise source and a noise figure analyser. If the noise source generates a noise power N_0 when off, and $N_H = \alpha N_0$ when on, and the ratio Y of the noise powers is measured, the noise factor can be determined as

$$F = \frac{\alpha - 1}{Y - 1} = \frac{ENR}{Y - 1}, \tag{8}$$

where $ENR = \alpha - 1$ is the excess noise ratio (ENR) of the switchable noise source. For a sequence of N devices, with noise factors $F_1, F_2, \cdots, F_N$ and gains $G_1, G_2, \cdots, G_N$, the total gain is $G = G_1 \cdot G_2 \cdots G_N$ and the total noise factor is[37]

$$F = F_1 + \frac{F_2 - 1}{G_1} + \frac{F_3 - 1}{G_1 G_2} + \cdots + \frac{F_N - 1}{G_1 G_2 \cdots G_{N-1}}. \tag{9}$$

By measuring the gain and noise factor of the system as it is built up, the noise figure of each element can be extracted in turn.

Rather than just obtaining the ratio Y, it is preferable to measure the noise spectra individually. Accordingly, we used an Agilent N1996A spectrum analyser to record spectra at 1001 points in the frequency range of 50–450 MHz, with a resolution bandwidth of 1 MHz, and a video bandwidth of 30 Hz. The noise was generated by a switchable noise generator (BBGEN[38]), which was switched on and off for alternate scans. Its ENR in the frequency range of the cables is approximately 15 dB when used with a 10 dB attenuator. The signal at the cable output was amplified using an HD24388 pre-amplifier[39] before being routed to the spectrum analyser. 2048 scans of each state were accumulated and their rms average taken. Two preliminary sets of measurements, first with the noise generator alone and then with the noise generator and pre-amp, were made to characterize the equipment. These allowed the noise figure for the spectrum analyser (~35 dB) and the gain and noise figure of the pre-amp (~25 dB and ~0.7 dB, respectively, in agreement with the specifications) to be established. The cable was then introduced, so the

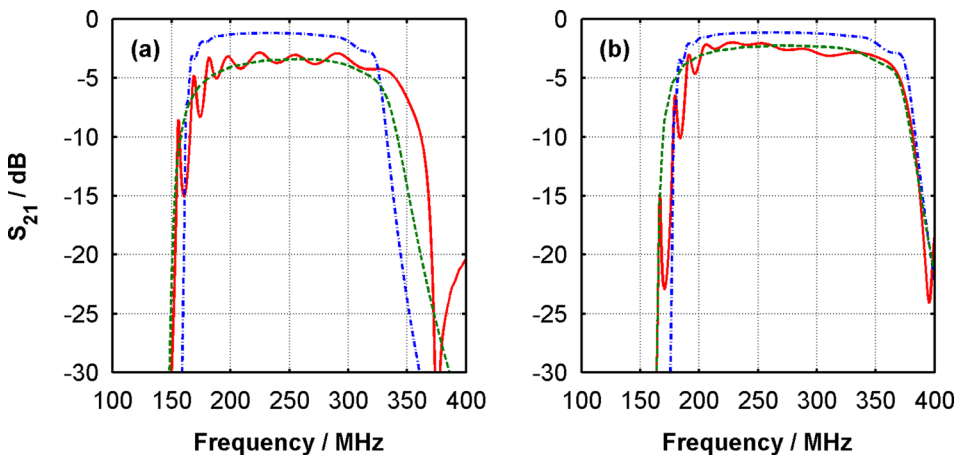

FIG. 3. S_{21} spectra (dB) for the MI cables: (a) cable 1, 80 mm loops; (b) cable 2, 70 mm loops. Red, full lines are measured spectra; blue, dashed-dotted lines are spectra calculated with the basic cable parameters; green, dashed lines are calculated with allowance for parasitic capacitance and dielectric loss.

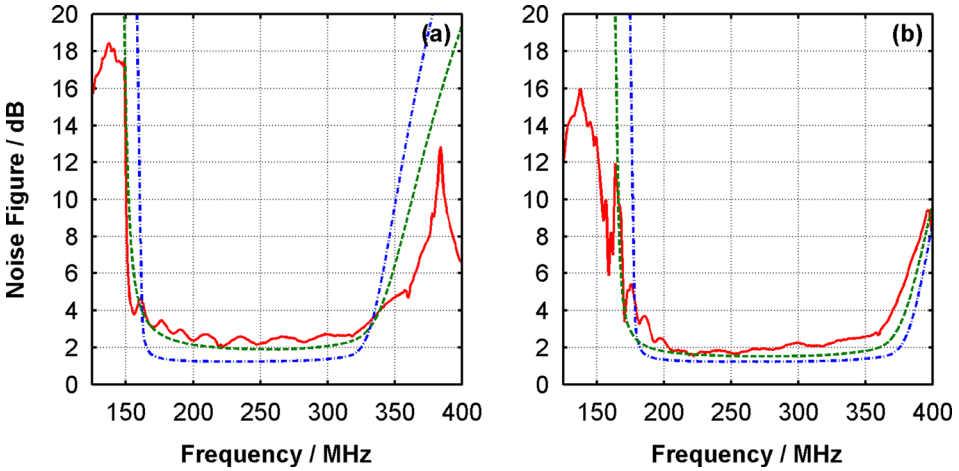

FIG. 4. Noise figure (dB) spectra for the two MI cables: (a) Cable 1, 80 mm loops; (b) Cable 2, 70 mm loops. Red, full lines are measured spectra; blue, dashed-dotted lines are spectra calculated with the basic cable parameters; green, dashed lines are calculated with allowance for parasitic capacitance and dielectric loss.

system contained the device under test. Following analysis, either using the Y-factors and the Friis cascade formula (9) or by direct calculation of the various noise spectra, the noise factor for the cable was extracted, and hence the noise figure found. These are shown in Figure 4 as the red lines and compared to the calculated values from (7) and (4) shown as the blue dashed-dotted lines.

The key point in these results is that there are no adjustable parameters in the calculations. The cable properties are fixed: the capacitance is simply the size of the surface-mount component attached to the circuits, and the loop inductance and resistance are obtained from measurements of the resonant frequency and Q-factor of single elements. The noise figure (6) is a ratio, so there are no scaling factors. The calculated noise figure over the useable frequency band is approximately 1.25 dB for both cables, which we can write as 1.45 dB/m in the low loss limit for comparison purposes. The measured values are 1.9 and 2.4 dB for the 70 mm and 80 mm cables, respectively, corresponding to 2.3 and 2.8 dB/m. As explained previously, this difference arises partly because there is parasitic capacitance between the loops that also introduces loss from the dielectric substrate; this effect is not included in the basic model. Nevertheless, for a calculation with no variable parameters, the agreement between the measured and calculated noise figures is pleasing. If we introduce the allowance for the parasitic capacitance as described for calculating the S-parameters and include a contribution to the noise from the loss in the parasitic capacitor, we obtain the green curves in Figure 4, which show a rather better match to the measured data.

IV. FUNDAMENTAL LIMITS

Although the modified circuit model is in good agreement with the measurements, it is clear that the losses and corresponding noise figures of MI cables are high. We now consider whether the origin of the loss can be understood and potentially reduced.

First, we emphasise that loss and noise are related. This is clear both from (1) which shows that all resistors generate noise, and more generally from the FDT.[26–28] This relates the fluctuations in a system at temperature T, with generalised coordinates X, acted on by generalised "force" F, to its generalised susceptibility χ, where $\chi = X/F$, through

$$\langle F^2 \rangle = 4k_B T \chi'', \tag{10}$$

where χ'' is the imaginary part of the susceptibility. Thus, the FDT links noise to loss. The fluctuations arise because when a "force" is applied at finite temperature, there is a continuum of states into which the system can move, whose probability of occupation is governed by Boltzmann statistics. Even when no "force" is applied, the system can lie in a range of states, and can even move between these states when in thermal equilibrium. Thus, there are fluctuations in X and hence F which manifest themselves as noise. Accordingly, we only need to review the loss mechanism in the cables: the noise figure will follow the loss.

We have already seen that the lowest attenuation in an MI cable occurs at resonance, when $k''a \approx 1/\kappa Q = R/2\omega_0 M$ and the impedance is $Z_{0MI} = \omega_0 M$. We can therefore write $k'' = R_s/2Z_{0MI}$, where R_s is the resistance per unit length of the cable and is given by $R_s = R/a$. In fact, all transmission lines have an attenuation constant of $k'' = R_s/2Z_0$ (Ref. 40), where R_s is the series resistance per unit length and Z_0 is the characteristic impedance, and we have ignored the shunt conductance. In this respect, MI cable is no different. We therefore compare it to two alternatives: a parallel wire and a coaxial cable, taking as the bench-mark the MI cable without parasitic capacitance and dielectric loss, i.e., the calculation based on the values in Table I that gives the blue lines in Figure 3, where the loss is 1.46 dB/m.

We first consider a parallel wire cable with comparable dimensions to the MI cable: a wire separation of 5 mm and a circumference equal to that of the 0.5 mm wide copper tracks in the MI cable, i.e., a diameter of 0.34 mm. We assume that these wires have the same resistance per unit length as the track in the MI cable of approximately 8.2 Ω/m, so the resistance per unit length of the parallel wire line would be 16.4 Ω/m. Furthermore, the characteristic impedance of a parallel wire transmission line is $Z_w = \pi^{-1} Z_0 \ln(D/r)$, where Z_0 is the impedance of free space, D is the wire spacing, and r is the wire radius: in this case, $Z_w = 405$ Ω. This leads to an attenuation of approximately 0.088 dB/m (compared to a value of 0.04 dB/m for commercially available 300 Ω cable, whose wire separation is significantly greater than here). Thus, the MI cable is some 16 times lossier than a comparable parallel wire line. This arises from two factors. First, the

characteristic impedance of the MI cable is 8 times smaller than that of the parallel wire line. Second, in the MI cable, the loops overlap by a factor of almost 2, so the MI cable has a resistance per unit length at least double that of a comparable parallel wire line. The 16-fold increase in attenuation of MI cable therefore has an entirely physical explanation.

Of course, we have deliberately designed the MI cable to have a characteristic impedance of 50 Ω, so it might be more appropriate to compare its performance with a 50 Ω coaxial cable. For this purpose, we consider RG178, which has a diameter of 1.8 mm, comparable to a catheter-mounted MI cable, and a loss of ~0.8 dB/m at 300 MHz.[41] This is still significantly better than the MI cable, primarily because the MI track length is two times greater as was the case for the parallel wire cable.

These factors inescapably makes the MI cable more lossy than continuous alternatives and cannot be reduced: we require large inter-loop coupling for effective propagation, and this requires large loop overlap, as has been shown previously.[20] To improve the MI cable performance, the track resistance must be reduced. This has been attempted using superconductors[42] with some degree of success. However, if superconductors were used to make conventional cables, they would still be less lossy than the MI equivalent.

The key property of the MI cable that makes it of value, despite its extra loss and noise, is the fact that it does not provide an electrically continuous connection. In cases where continuous wires cannot be used, such as in signal extraction from internal *in vivo* MRI, MI cables can provide a safe alternative.

V. CONCLUSIONS

In conclusion, we have measured the propagation losses and noise figures for two different magneto-inductive cables, and shown them to be poor compared to conventional cables. Fundamental explanations have been provided in terms of the series resistance and characteristic impedance. The former must typically be higher and the latter lower in MI cables. However, when a continuous cable cannot be used, the MI cable can provide a viable alternative, provided that the benefit obtained from using such a connector outweighs the extra noise penalty. This has indeed proved to be the case in internal MRI,[22] where the potential for improved imaging without compromising patient safety has been convincingly demonstrated.

ACKNOWLEDGMENTS

Support from the Leverhulme Trust through their award "Metamaterials and the Control of Electromagnetic Fields" is gratefully acknowledged.

[1]N. Tesla, "Apparatus for transmission of electrical energy," U.S. patent 649621 (15 May 1900).
[2]A. Kurs *et al.*, "Wireless power transfer via strongly coupled magnetic resonances," Science **317**(5834), 83–86 (2007).
[3]Z. Sun and I. F. Akyildiz, "Magnetic induction communications for wireless underground sensor networks," IEEE Trans. Antennas Propag. **58**(7), 2426–2435 (2010).
[4]Z. Sun *et al.*, "Increasing the capacity of magnetic induction communications in RF-challenged environments," IEEE Trans. Commun. **61**(9), 3943–3952 (2013).
[5]W. X. Zhong, C. K. Lee, and S. Y. R. Hui, "General analysis on the use of Tesla's resonators in domino forms for wireless power transfer," IEEE Trans. Ind. Electron. **60**(1), 261–270 (2013).
[6]E. Shamonina *et al.*, "Magnetoinductive waves in one, two, and three dimensions," J. Appl. Phys. **92**(10), 6252–6261 (2002).
[7]E. Shamonina *et al.*, "Magneto-inductive waveguide," Electron. Lett. **38**(8), 371–373 (2002).
[8]J. I. Agbinya and M. Masihpour, "Excitation methods for magneto inductive waveguide communication systems," in *Fifth International Conference on Broadband and Biomedical Communications (IB2Com)* (2010), pp. 1–6.
[9]J. B. Pendry *et al.*, "Low frequency plasmons in thin-wire structures," J. Phys.: Condens. Matter **10**(22), 4785–4809 (1998).
[10]J. B. Pendry *et al.*, "Extremely low frequency plasmons in metallic mesostructures," Phys. Rev. Lett. **76**(25), 4773–4776 (1996).
[11]J. B. Pendry *et al.*, "Magnetism from conductors and enhanced nonlinear phenomena," IEEE Trans. Microwave Theory Tech. **47**(11), 2075–2084 (1999).
[12]W. N. Hardy and L. A. Whitehead, "Split-ring resonator for use in magnetic-resonance from 200-2000 MHz," Rev. Sci. Instrum. **52**(2), 213–216 (1981).
[13]M. C. K. Wiltshire *et al.*, "Microstructured magnetic materials for RF flux guides in magnetic resonance imaging," Science **291**(5505), 849–851 (2001).
[14]C. Kittel, in *Introduction to Solid State Physics*, 4th ed. (John Wiley & Sons, 1971).
[15]M. C. K. Wiltshire *et al.*, "Dispersion characteristics of magneto-inductive waves: Comparison between theory and experiment," Electron. Lett. **39**(2), 215–217 (2003).
[16]M. C. K. Wiltshire *et al.*, "Experimental and theoretical study of magneto-inductive waves supported by one-dimensional arrays of "swiss rolls"," J. Appl. Phys. **95**(8), 4488–4493 (2004).
[17]R. R. A. Syms, E. Shamonina, and L. Solymar, "Magneto-inductive waveguide devices," IEE Proc. Microwaves Antennas Propag. **153**(2), 111–121 (2006).
[18]J. Agbinya, "A magneto-inductive link budget for wireless power transfer and inductive communication systems," Prog. Electromagn. Res. C **37**, 15–28 (2013).
[19]B. Gulbahar and O. B. Akan, "A communication theoretical modeling and analysis of underwater magneto-inductive wireless channels," IEEE Trans. Wireless Commun. **11**(9), 3326–3334 (2012).
[20]R. R. A. Syms *et al.*, "Thin-film magneto-inductive cables," J. Phys. D: Appl. Phys. **43**(5), 055102 (2010).
[21]R. R. A. Syms and L. Solymar, "Bends in magneto-inductive waveguides," Metamaterials **4**(4), 161–169 (2010).
[22]R. R. A. Syms *et al.*, "Magneto-inductive catheter receiver for magnetic resonance imaging," IEEE Trans. Biomed. Eng. **60**(9), 2421–2431 (2013).
[23]R. R. A. Syms *et al.*, "Magnetic resonance imaging using linear magneto-inductive waveguides," J. Appl. Phys. **112**(11), 114911 (2012).
[24]J. B. Johnson, "Thermal agitation of electricity in conductors," Phys. Rev. **32**(1), 97–109 (1928).
[25]H. Nyquist, "Thermal agitation of electric charge in conductors," Phys. Rev. **32**(1), 110–113 (1928).
[26]H. B. Callen and R. F. Greene, "On a theorem of irreversible thermodynamics," Phys. Rev. **86**(5), 702–710 (1952).
[27]H. B. Callen and T. A. Welton, "Irreversibility and generalized noise," Phys. Rev. **83**(1), 34–40 (1951).
[28]R. Kubo, "The fluctuation-dissipation theorem," Rep. Prog. Phys. **29**(1), 255 (1966).
[29]R. R. A. Syms and L. Solymar, "Noise in metamaterials," J. Appl. Phys. **109**(12), 124909 (2011).
[30]R. R. A. Syms, O. Sydoruk, and L. Solymar, "Noise in one-dimensional metamaterials supporting magnetoinductive lattice waves," Phys. Rev. B **87**(15), 155155 (2013).
[31]C. J. Stevens *et al.*, "Magnetic metamaterials as 1-D data transfer channels: An application for magneto-inductive waves," IEEE Trans. Microwave Theory Tech. **58**(5), 1248–1256 (2010).
[32]M. C. K. Wiltshire and R. R. A. Syms, "Measuring trapped noise in metamaterials," J. Appl. Phys. **115**(8), 084905 (2014).
[33]E. Shamonina and L. Solymar, "Magneto-inductive waves supported by metamaterial elements: Components for a one-dimensional waveguide," J. Phys. D: Appl. Phys. **37**(3), 362–367 (2004).
[34]R. R. A. Syms, L. Solymar, and I. R. Young, "Broadband coupling transducers for magneto-inductive cables," J. Phys. D: Appl. Phys. **43**(28), 285003 (2010).

[35]Claydon Ltd, Willenhall, West Midlands, UK.
[36]R. Syms and T. Floume, "Electric coupling in strongly coupled magneto-inductive cable," in *Proceedings of 7th International Congress on Advanced Electromagnetic Metamaterials in Microwaves and Optics, Bordeaux, France,* 2013, pp. 16–21.
[37]H. T. Friis, "Noise figures of radio receivers," Proc. IRE **32**(7), 419–422 (1944).
[38]Continental Compliance Ltd, 27 Weelsby Way, Hessle, East Yorkshire, HU13 0JN, UK.
[39]HD Communications Corp., 2180 Fifth Avenue, Unit 4, Ronkonkoma, NY 11779, USA.
[40]B. Bleaney and B. I. Bleaney, in *Electricity and Magnetism*, 3rd ed. (Oxford University Press, 1976).
[41]See http://www.caledonian-cables.net/product/Coaxial%20Cables/Mininature%20Coaxial%20Cables/RG178%20Mini-Coax.htm for mechanical and electrical characteristics and attenuation vs. frequency data.
[42]C. Kurter, J. Abrahams, and S. M. Anlage, "Miniaturized superconducting metamaterials for radio frequencies," Appl. Phys. Lett. **96**(25), 253504 (2010).